RSC Advances

PAPER

View Article Online
View Journal | View Issue

Cite this: *RSC Adv.*, 2023, **13**, 19403

Preparation of a highly functionalized activated carbon from waste third-monomer pressure filter liquid for removal of methylene blue in aqueous solution

Dingdan Tian, Yongjun Liu* and Bing Sun

Third monomer dimethyl isophthalate-5-sodium sulfonate (SIPM) is an additive widely used to modify polyester chips. During the manufacture of SIPM, large amounts of waste third-monomer pressure filter liquid are produced. As the liquid contains lots of toxic organics and highly concentrated Na_2SO_4, it will cause serious environmental pollution if discharged directly. In this study, highly functionalized activated carbon (AC) was prepared by directly carbonizing the dried waste liquid under ambient pressure. Structural and adsorption properties of the prepared AC were analyzed and evaluated by X-ray diffraction (XRD), scanning electron microscopy (SEM), Fourier transform infrared (FT-IR) spectroscopy, X-ray photoelectron spectroscopy (XPS), N_2 adsorption–desorption analysis and methylene blue (MB) as the adsorbate, respectively. Results showed that the adsorption capacity of the prepared AC to MB reached the highest when carbonization was conducted at 400 °C. XRD analysis showed that the AC has a disordered graphite-like crystal structure. FT-IR and XPS analyses showed that there were plenty of carboxyl and sulfonic functional groups in the AC. The adsorption follows the pseudo-second-order kinetic model and the isotherm process is consistent with the Langmuir model. The adsorption capacity increased with increasing solution pH and dropped when the solution pH exceeded 12. Increasing solution temperature favors the adsorption, where the maximum value can reach as high as 2816.4 mg g^{-1} at 45 °C, more than double the values reported to date. The adsorption of MB on the AC is mainly controlled by the electrostatic interaction between MB and the anionic form of carboxyl and sulfonic groups.

Received 4th April 2023
Accepted 20th June 2023

DOI: 10.1039/d3ra02216a

rsc.li/rsc-advances

1 Introduction

5-Sodium sulfodimethyl isophthalate (SIPM), commonly known as the third monomer, is a benzene derivative. SIPM plays an important role in improving the dyeing properties of polyester products.[1] During the production of SIPM, a large amount of waste pressure filter liquid is generated, which contains a large amount of sodium sulfate, sodium isophthalate-5-sulfonic acid (5-SSIPA), sodium monomethyl isophthalate-5-sulfonic acid (SSPM), and other unknown organics. If discharged directly without treatment, it will cause serious pollution to water bodies.[2]

At present, some enterprises just dilute the waste liquid before carrying on the biological treatment.[3] However, diluting does not decompose the pollutant but increases volume of the waste liquid. Yang *et al.*[4] attempted to recover 5-SSIPA from the waste liquid by liquid–liquid extraction. Liquid–liquid extraction bears the advantages of high efficiency and low equipment investment, but suffers secondary pollution and difficulty to meet the discharge standard. Macroporous resin[5] was also employed to recover the valuable products from this kind of liquid. As all the above processes suffer the process complexity or high costs, it is imperative to find efficient process to treat such waste.[6]

Recently, interest in preparing low cost adsorbents from various waste materials has grown enormously.[7] Marrakchi *et al.*[8] prepared mesoporous-activated carbon from chitosan flakes *via* single-step sodium hydroxide activation for the adsorption of methylene blue (MB), with a maximum adsorption capacity 143.53 mg g^{-1} at 50 °C. Sukhbaatar *et al.*[9] reported a metal-free high-adsorption-capacity adsorbent derived from spent coffee grounds for the removal of MB from aqueous solution and an adsorption capacity of 499.9 mg g^{-1} for MB was achieved. Khanday *et al.*[10] investigated efficient antibiotic cephalexin removal by activated carbon (AC) derived from a single-step pyrolysis of phosphoric acid-activated chitin and a monolayer capacity of 245.19 mg g^{-1} at 50 °C was obtained. Mohamed *et al.*[11] got a low cost carbonaceous hydrochar

College of Environmental Science & Engineering, Dalian Maritime University, Dalian, 116026, P. R. China. E-mail: lyjglow@dlmu.edu.cn; Fax: +86-411-84727670; Tel: +86-411-84725275

adsorbent from cellulose and lignin derived from rice straw, where monolayer adsorption capacity of 100 mg g^{-1} towards MB dye was reached. Other promising adsorbents with exceptional adsorption properties are being increasingly reported.[12]

Considering the organic matter in the waste third-monomer pressure filter liquid is rich in sulfonic acid and carboxyl groups, in the present study, carbonization was applied to prepare functionalized AC using this kind of liquid without the introduction of extra groups.[13] In addition, absorption properties of the prepared AC on cationic dye MB were evaluated. Adsorption kinetics, isotherms, and thermodynamics of the adsorption were performed. The maximum adsorption capacity of the prepared AC on MB is 2816.4 mg g^{-1}. This study is of great significance for recycling highly concentrated organic waste liquid, saving resources and reducing environmental load.

2 Materials and methods

2.1 Materials

The waste liquid produced in the production process of SIPM was obtained from an enterprise in Shandong Province, China. Its composition is: water (46.9%), organic matter (39.1%) and Na_2SO_4 (4.0%).

Hydrochloric acid (HCl) and sodium hydroxide (NaOH) were purchased from Tianjin Zhiyuan Chemical Reagent Co., Ltd and Tianjin Kemeiou Chemical Reagent Co., Ltd, respectively. MB was provided by Sinopharm Chemical Reagent Co., Ltd.

2.2 Preparation of AC

100 mL of the waste liquid was put into an oven dryer at 105 °C to dry to constant weight (about 53.0 g). 5.0 g of the dried sample was calcined in a Muffle furnace for 2 h at certain temperature in the range 200–800 °C. It should be noted that the carbonization should be conducted in a well-ventilated laboratory, because a large amount of gases would be liberated during carbonization. When the temperature of muffle furnace dropped to room temperature, it was taken out and ground to powder.

After weighing, the powdered sample was washed with deionized water until the electrical conductivity of the washing solution remained unchanged.

2.3 Adsorption experiment

The adsorption performance under different pH values (2–14) was explored. MB solution (500.0 mg L^{-1}, 60 mL) was poured into a 150 mL conical flask, and sodium hydroxide (1.0 mol L^{-1}) and hydrochloric acid (1.0 mol L^{-1}) solutions were applied to regulate the pH of the solution to the expected value. AC (15 mg) were added to the solution under shaking (150 rpm, 25 °C). The adsorption kinetics of MB (500.0 mg L^{-1}) was examined at pH = 12.0 and temperature 25 °C. Adsorption isotherm of MB (pH = 12.0) was studied under different adsorption temperatures (25–45 °C), where the initial concentration of MB was in the range 400–800 mg L^{-1}. All adsorption experiments were repeated twice.

The equilibrium adsorption capacity (Q_e (mg g^{-1})) of MB is defined by eqn (1):

$$Q_e = \frac{(C_0 - C_e)V}{m} \quad (1)$$

where V is the volume of MB solution (L); C_0 and C_e are the initial and the equilibrium concentration of MB (mg L^{-1}); and m is the mass of AC (g).

Pseudo-first-order kinetic model and pseudo-second-order kinetic model[14] are used to describe the adsorption process as eqn (2) and (3), respectively:

$$\ln(Q_e - Q_t) = \ln Q_e - k_1 t \quad (2)$$

$$\frac{t}{Q_t} = \frac{1}{k_2 Q_e^{\,2}} + \frac{t}{Q_e} \quad (3)$$

where Q_t is adsorption amount of AC (mg g^{-1}) at time t (min); k_1: is adsorption rate constant of the pseudo-first-order kinetic model (min^{-1}); and k_2: is adsorption rate constant of the pseudo-second-order kinetic model (g (mg^{-1} min^{-1})).

Langmuir model[15] and Freundlich model[16] are employed as the isothermal processes as eqn (4) and (5):

$$\frac{C_e}{Q_e} = \frac{C_e}{Q_m} + \frac{1}{k_L Q_m} \quad (4)$$

$$\ln Q_e = \ln K_F + \frac{1}{n}\ln C_e \quad (5)$$

where, Q_m: the maximum adsorption capacity of the AC (mg g^{-1}); n: the Freundlich constant; K_L and K_F: the constant corresponding to the energy of sorption (L mg^{-1}) and adsorption performance (mg g^{-1} (L mg^{-1})$^{1/n}$), respectively.

To further explore the thermodynamic changes in the adsorption process, three parameters were calculated: Gibbs free energy ΔG (kJ mol^{-1}), entropy ΔS (J (mol^{-1} K^{-1})), and enthalpy ΔH (kJ mol^{-1}). The calculation formulas are as follows:[17,18]

$$\Delta G = \Delta H - T\Delta S \quad (6)$$

$$K_c = \frac{C_{Ae}}{C_e} \quad (7)$$

$$\ln K_c = \frac{-\Delta H}{RT} + \frac{\Delta S}{R} \quad (8)$$

where, T: the adsorption temperature (K); C_{Ae} and C_e: equilibrium concentrations of MB in AC and AC in solution (mg L^{-1}); R: the universal gas constant (8.314 J mol^{-1} K^{-1}).

2.4 Characterization of AC

Scanning electron microscope (SEM) was applied to analyze the surface topography. X-ray diffraction (XRD) patterns of the prepared AC were examined by a Rigaku D/Max-Ultima+ diffractometer equipped with Kα radiation of Cu (λ = 0.15418 nm). Fourier transform infrared spectrometry (FT-IR) was applied to analyze the functional group. The change of binding energy was measured by X-ray photoelectron spectroscopy (XPS). N_2 adsorption–desorption isotherm was measured at 77

K on a Micromeritics ASAP 2460 adsorption analyzer. UV-Vis spectrophotometry was used to determine the concentration of MB (wavelength: 664 nm, detection limit: 0.01 mg L^{-1}).

3 Results and discussion

3.1 Effect of carbonization temperature on the yield and adsorption performance of AC

The effect of carbonization temperature on the yield of AC is shown in Fig. 1(a). It can be noted from Fig. 1 that when the carbonization temperature is lower than 400 °C, no AC is formed. The yield of AC increased with increasing carbonization temperature in the range 400–550 °C and decreased when the carbonization temperature is in the range 550–650 °C. When the carbonization temperature exceeded 650 °C, no AC was obtained, indicating the formed AC decomposed at high temperature.

In order to optimize the carbonization temperature, adsorption capacities of the AC on MB obtained at different carbonization temperatures were given in Fig. 1(b). Fig. 1(b) shows that the adsorption capacity of the prepared AC decreased with the increasing carbonization temperature. The adsorption capacity decreased from a maximum of 1244.8 mg g^{-1} to 136.7 mg g^{-1} when the carbonization temperature increased from 400 °C to 650 °C. Such phenomenon can be explained that carboxyl group will be lost at high carbonization temperature. Such a carbonization temperature dependence is very beneficial in industrial applications, because energy cost would be greatly reduced in producing the AC at lower carbonization temperature. Therefore, AC prepared at calcining temperature of 400 °C (AC-400) was used for the following study.

3.2 Characterizations of AC-400

SEM images of AC-400 are presented in Fig. 2. It can be shown in Fig. 2 that the AC-400 has a rough, puffy surface and pore structure with different pore sizes, this is because gaseous products were generated during the preparation of AC-400.

Fig. 3(a) shows the XRD patterns of the prepared AC-400. As shown in Fig. 3, AC-400 has a strong diffraction peak at $2\theta = 22°$, corresponding to the (002) crystal plane of graphite. The weak diffraction peak at $2\theta = 43°$ corresponds to the (100) crystal plane of graphite.[19–21] This indicates that AC-400 has a disordered graphite-like crystal structure.[18,19]

FT-IR spectra of AC-400 are presented in Fig. 3(b). The strong and broad band centered at 3440 cm^{-1} corresponds to the

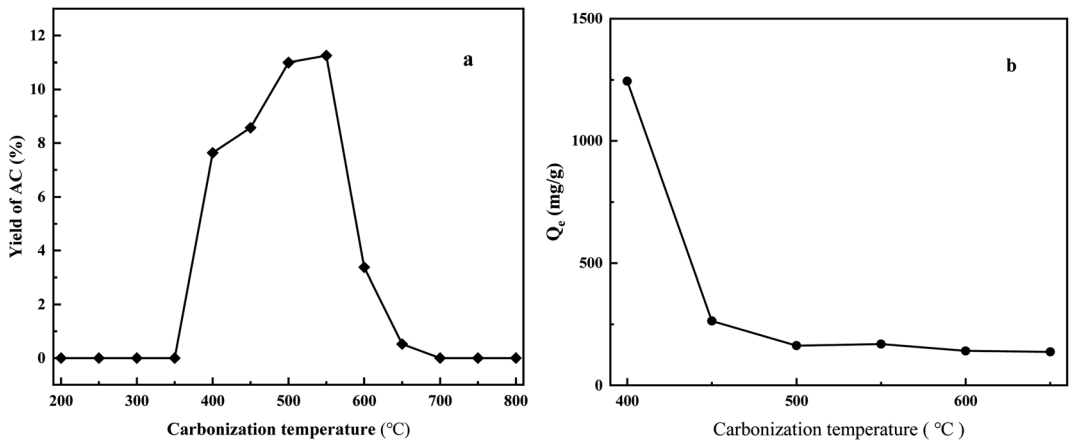

Fig. 1 Effect of carbonization temperature on (a) yield and (b) adsorption capacity of AC.

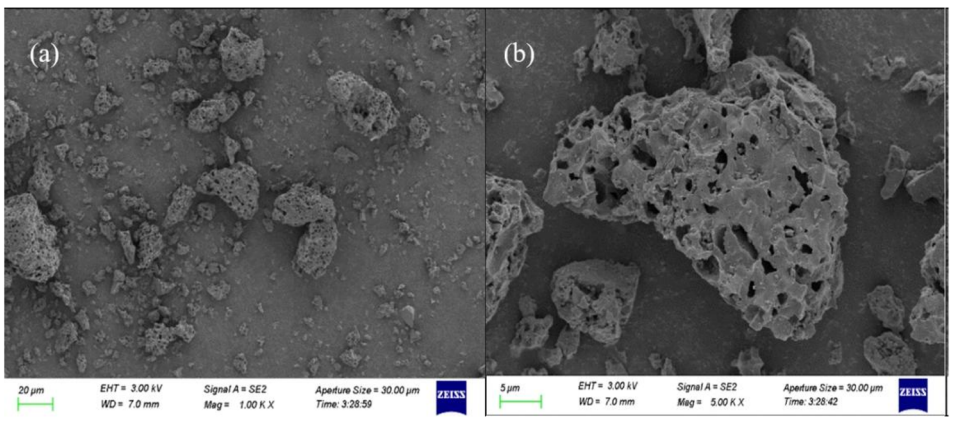

Fig. 2 SEM images of AC-400 ((a) magnification = 1.00 kX; (b) magnification = 5.00 kX).

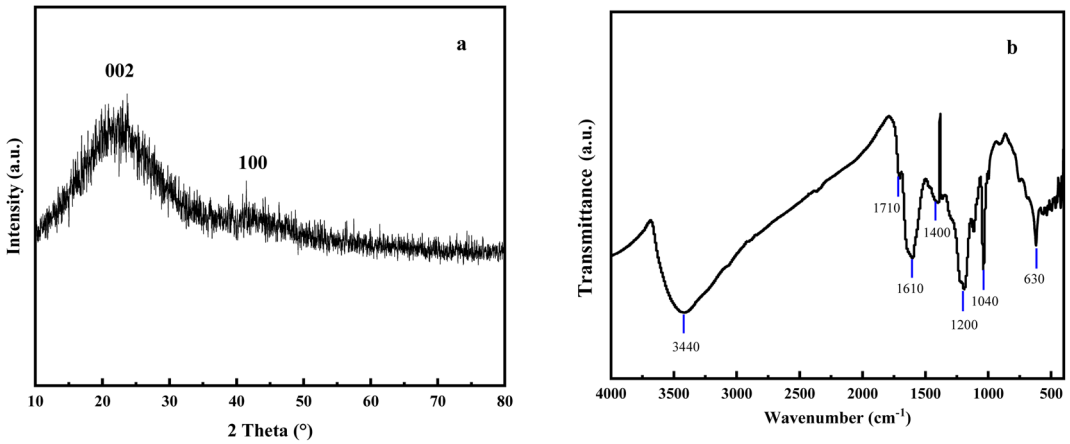

Fig. 3 XRD pattern (a) and FT-IR spectra (b) of AC-400.

stretching vibration of O–H of carboxylic group.[22] The peaks at 1710, 1610 cm^{-1} could be assigned to C=O stretch of carboxylic acid group.[23] The absorption peak at 1200 cm^{-1} is attributed to the stretch of C–O group.[24] The band at 1040 cm^{-1} is C–H deformation vibration.[25] The peak appeared at around 630 cm^{-1} could be assigned to the S–O stretching vibration.[21] The presence of both C–O and C=O indicate that there is carboxylic acid functional groups (–COOH) in AC-400, which may adsorb cationic dyes in the solution.[26] The evident vibration peaks of S–O proved that AC-400 contain sulfonic group ($–SO_3H$).

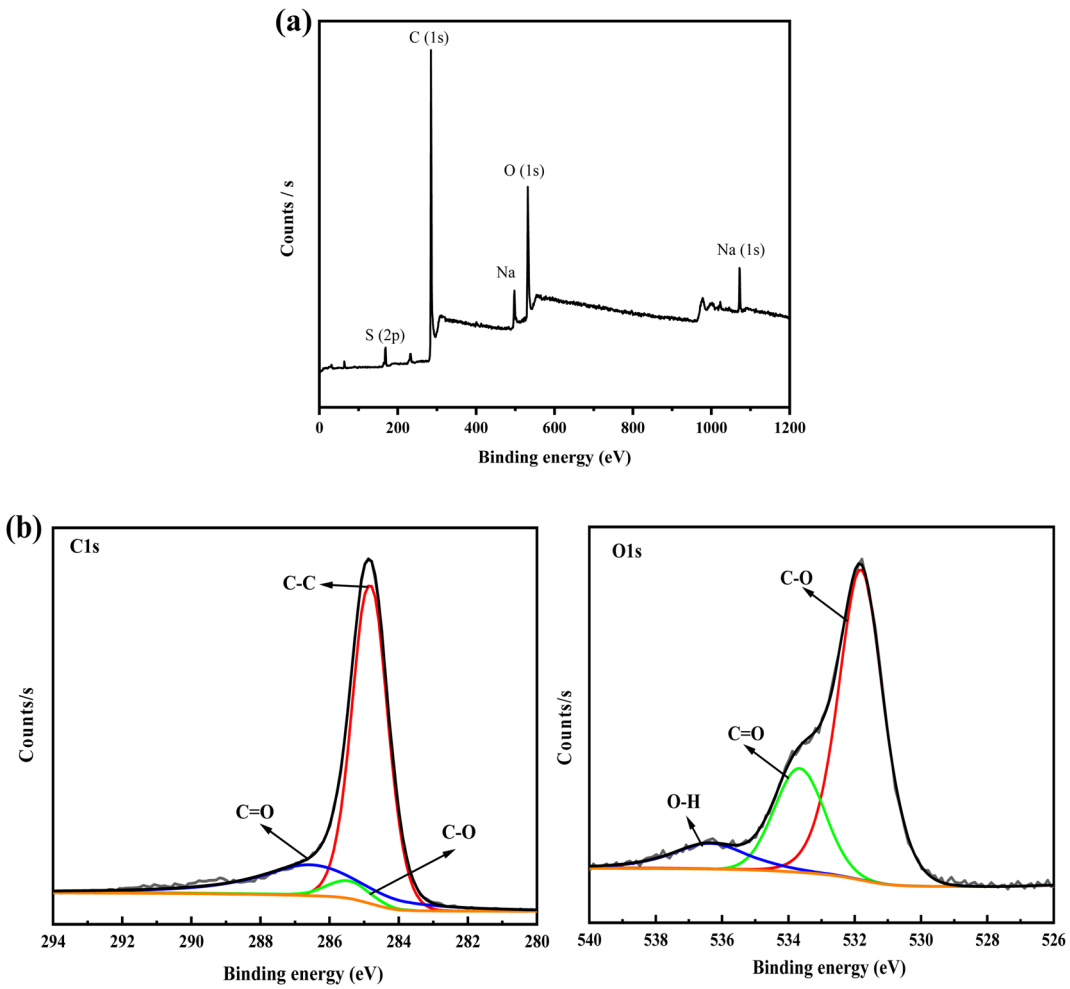

Fig. 4 Wide scan XPS spectra (a) and C1s and O1s high resolution XPS spectra (b) of AC-400.

Wide scan and C1s and O1s high resolution XPS spectra of AC-400 are shown in Fig. 4(a) and (b), respectively. Fig. 4(a) shows that AC-400 is mainly composed of carbon and oxygen as well as a small amount of sulfur and sodium. These are the main components from the organic matter existing in the waste dried third-monomer press filtration liquid. C1s band of AC-400 can be deconvoluted into three peaks with binding energies of 286.7, 285.4 and 284.7 eV, indicating the existence of C═O, C–O and C–C,[27–29] respectively. O1s band of AC-400 can also be deconvoluted into three peaks: O–H (536.4 eV), O═C (533.7 eV) and O–C (531.8 eV).[30] In summary, the surface of AC-400 contains a certain amount of oxygen-containing functional groups such as C–O, C═O and O–H, which is consistent with those of the FT-IR analysis.

Fig. 5 shows the adsorption–desorption isotherm of nitrogen gas onto the AC-400 at −196 °C. It can be inferred from Fig. 5 that the surface area of AC-400 is very small (2.25 $m^2 g^{-1}$), which is contradictory to its excellent adsorption performance. Possible reasons may be due to its high density of the acidic functional groups, which provides good access by MB in solution to these functional groups, giving rise to its high adsorption performance.[31]

3.3 Adsorption performance of AC-400

Dependence of adsorption capacity of AC-400 on the solution pH is shown in Fig. 6. It can be observed from Fig. 6 that adsorption capacity of AC-400 increases with increasing solution pH in the range of pH 2–12 and decreases when the pH exceeds 12. The adsorption capacity of AC-400 increased from 1028.7 to 1581.9 mg g^{-1} when the solution pH increased from 2 to 12. However, the adsorption capacity decreased from 1581.9 mg g^{-1} to 657.9 mg g^{-1} when pH increased from 12 to 14. Such phenomena can be explained by the fact that AC-400 has numerous –SO_3H and –COOH groups on its surface. When the solution pH is low, only –SO_3H is in the anionic form, which will attract the cationic dye MB by static electrical forces. With the increase of pH, more and more –COOH was dissociated into COO^- and more MB will be adsorbed onto the AC-400 surface

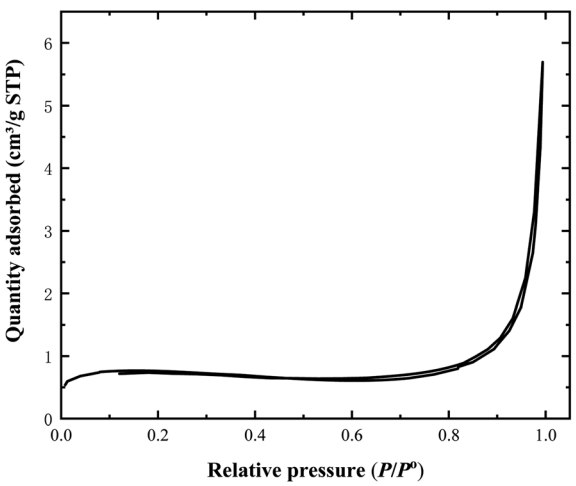

Fig. 5 N_2 adsorption–desorption isotherm of AC-400 at −196 °C.

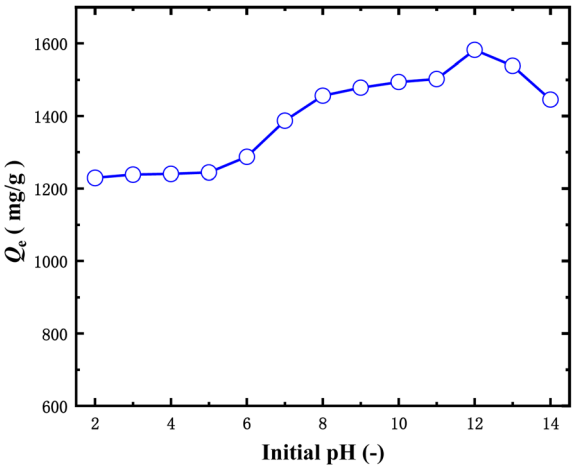

Fig. 6 Effect of initial solution pH on the absorption capacity of AC-400.

and the adsorption capacity of the AC-400 increased. At high pH, there will be a large number of sodium ions in the solution, which will compete with the cationic dye MB for AC-400, resulting in a decrease in adsorption capacity. As a result, AC-400 has the highest adsorption capacity at pH 12.

The adsorption amount of AC-400 to MB with adsorption time was shown in Fig. 7(a). It can be found from Fig. 7(a) that the adsorption amount increased rapidly in the first 20 min and then increased slowly between 20 and 40 min and increased little when he adsorption time was more than 40 min. Therefore, 40 min can be enough for getting adsorption equilibrium.

Two kinetic models, pseudo-first-order and pseudo-second-order, were used to describe the present adsorption processes. Kinetic parameters and correlation coefficients are listed in Table 1.

Table 1 demonstrated that the correlation coefficient of the pseudo-second-order kinetic model is higher (0.99) that of the pseudo-first-order kinetic model. Therefore, the adsorption process of AC-400 on MB is more consistent with the pseudo-second-order kinetics. In addition, the equilibrium adsorption capacity calculated by the pseudo-second-order kinetic model is 1510.4 mg g^{-1}, which is very close to that observed in the experimental results. Therefore, this model was consistent with the adsorption process of MB for AC, indicating that a chemical bond was formed between MB and AC-400.[32,33]

Fig. 8(a) showed the effects of initial MB concentration and adsorption temperature on the adsorption capacity of AC-400. It can be observed that Fig. 8(a) the adsorption capacity increases with both increase of the initial MB concentration and the adsorption temperature. When the initial MB concentration increased from 400 to 800 mg L^{-1}, the adsorption capacity of AC-400 increased from 1375.8 to 2418.5 mg g^{-1} (45 °C). High initial MB concentration increases the effective contact area with the AC-400 and provides necessary driving force to overcome the resistance to the mass transfer of MB on interface which increases the adsorption capacity.[21] When the adsorption temperature increased from 25 °C to 45 °C, the adsorption

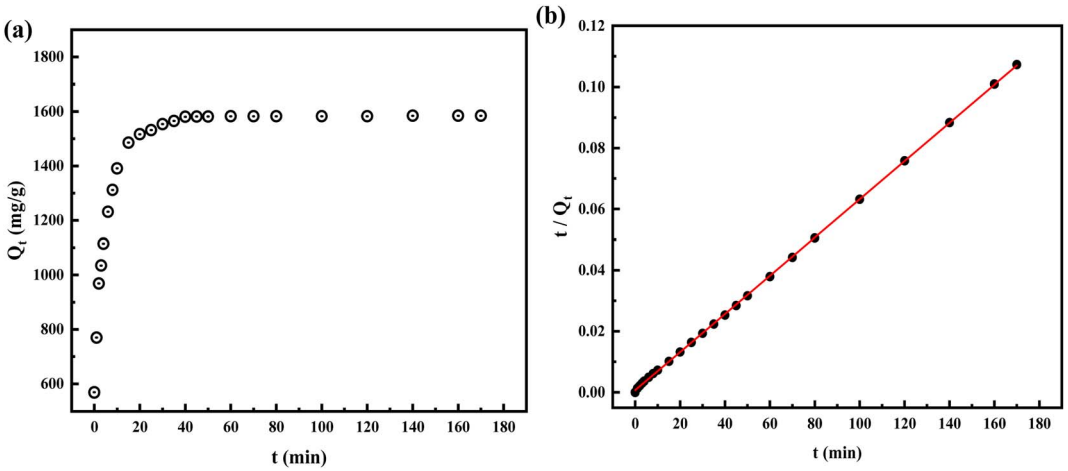

Fig. 7 Effect of adsorption time on adsorption capacity of AC-400 (a); and pseudo-second-order kinetic fitting (b).

Table 1 Adsorption kinetic parameters of MB over AC-400

Pseudo-first-order model			Pseudo-second-order model		
k_1 (min^{-1})	Q_e (mg g^{-1})	R^2	k_2 (g (mg^{-1} min^{-1}))	Q_e (mg g^{-1})	R^2
0.12	510	0.98	7.0×10^{-4}	1510.4	0.99

capacity of AC-400 to MB increased from 2179.3 to 2418.5 mg g^{-1}. This may be that the high solution temperature favors the dissociation of –COOH group, where more anionic species were formed, resulting the higher adsorption capacity.[34]

Fig. 8(b) and (c) showed the fittings of Langmuir and Freundlich adsorption isotherms of AC-400, respectively.

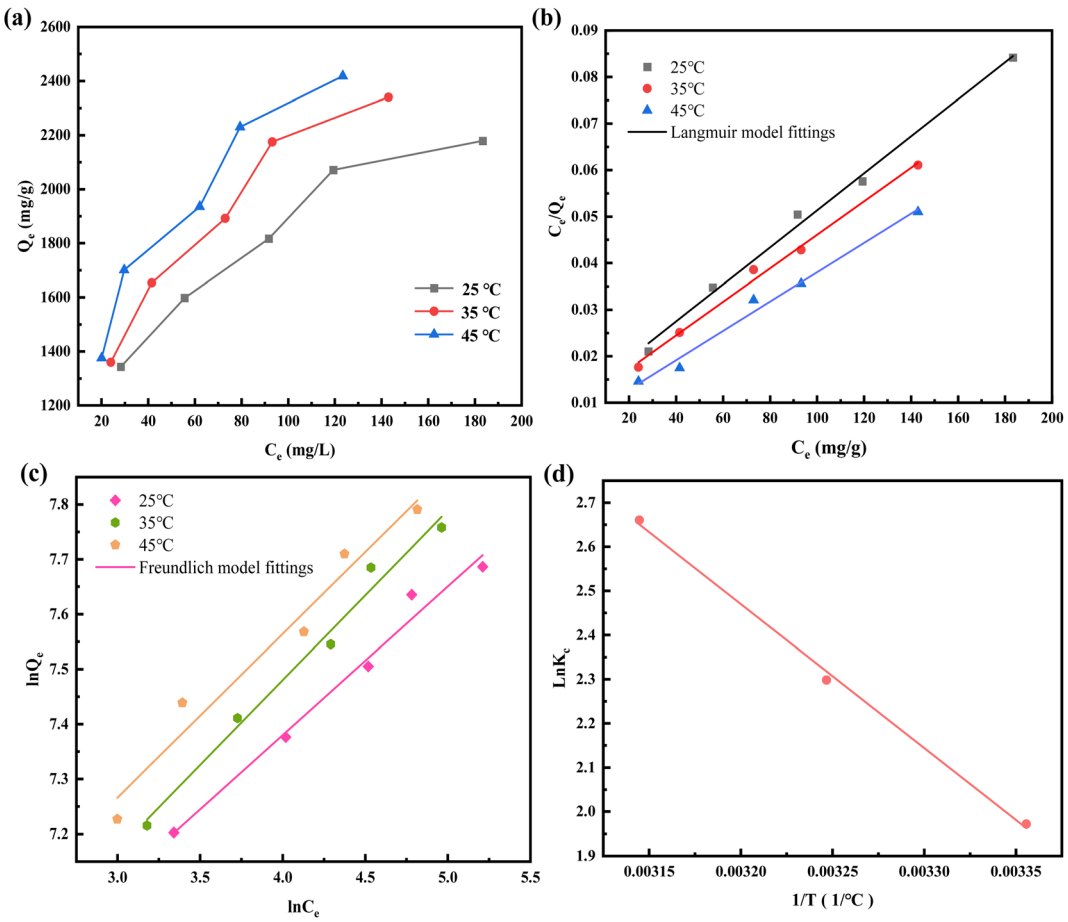

Fig. 8 Effect of initial MB concentration and adsorption temperature on adsorption capacity (a), Langmuir adsorption isotherm model fitting (b), Freundlich adsorption isotherm model fitting (c) and van't Hoff diagram (d) of AC-400.

Table 2 Langmuir and Freundlich constants for the removal of MB over the prepared AC-400

Temperature (°C)	Langmuir adsorption isotherm			Freundlich adsorption isotherm		
	Q_m (mg g^{-1})	K_L (L mg^{-1})	R^2	n	K_F (L g^{-1})	R^2
25	2513.2	0.03	0.99	3.70	543.4	0.97
35	2775.6	0.04	0.99	3.24	515.2	0.97
45	2816.4	0.05	0.98	3.36	585.4	0.95

Table 3 Comparison of adsorption capacity of various adsorbents for MB

Adsorbents	T (°C)	q_{max} (mg g^{-1})	Reference
AC-400	45	2816.4	This study
AC-400	25	2513.2	This study
Honeycomb-like cork activated carbon	50	1284.0	36
Fox nutshell activated carbon	30	968.7	37
Rice husk activated carbon	25	476.2	38
Sludge and coconut shell activated carbon	20	602.8	39

Parameters calculated from the linear forms of the two isotherms are summarized in Table 2.

It can be observed from Table 2 that the adsorption was in better agreement with the Langmuir adsorption isotherm than Freundlich one according to the value of R^2, suggesting that the adsorption of MB belongs to single layer adsorption type.[35] In addition, the Langmuir fitting results showed that the maximum adsorption capacity of AC-400 can reach 2816.4 mg g^{-1} at 45 °C, which is much higher than those prepared from other raw materials (Table 3).

van't Hoff plot for the adsorption process of AC-400 is shown in Fig. 8(d) and the thermodynamic parameters calculated are summarized in Table 4. Negative values of ΔG showed that the adsorption is a spontaneous process. ΔG values decreased with increasing solution temperature, indicating that high temperature is favorable for the adsorption. Positive ΔH values confirmed the MB adsorption on AC-400 is endothermic. The positive value of ΔS suggested an increased randomness at solid/solution interface during the adsorption. In summary, the adsorption of MB by AC-400 is a spontaneous and endothermic process.

Table 4 Thermodynamic parameters of AC-400 for MB adsorption

Adsorption temperature (K)	ΔG (KJ mol^{-1})	ΔS (J mol^{-1} K^{-1})	ΔH (KJ mol^{-1})
298	−70.35	1.55	392.02
308	−85.86		
318	−101.38		

3.4 Adsorption mechanism of AC-400 for MB

In order to better understand the adsorption process, UV-Vis spectra of MB solution (C_0, 800 mg L^{-1}) and FTIR spectra of

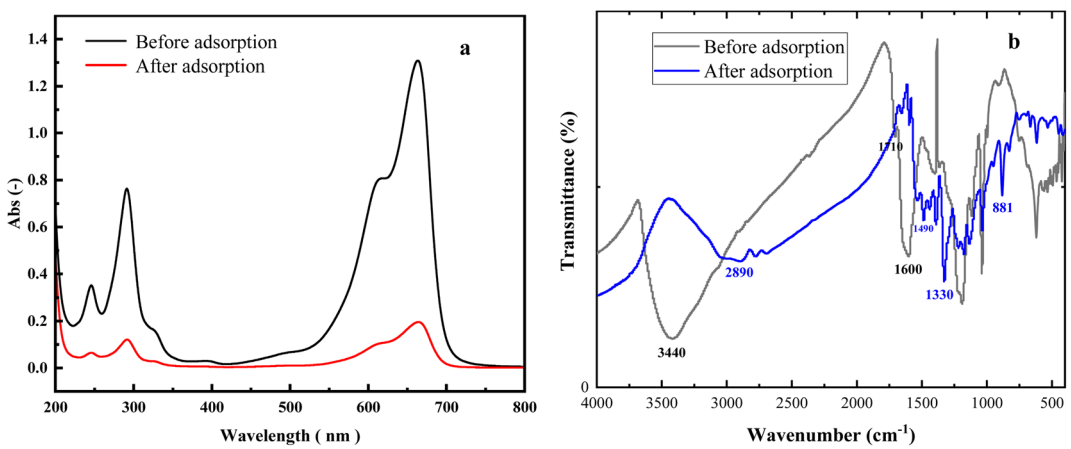

Fig. 9 UV-Vis spectra of MB solution (a) and FTIR spectra of AC-400 (b) before and after adsorption.

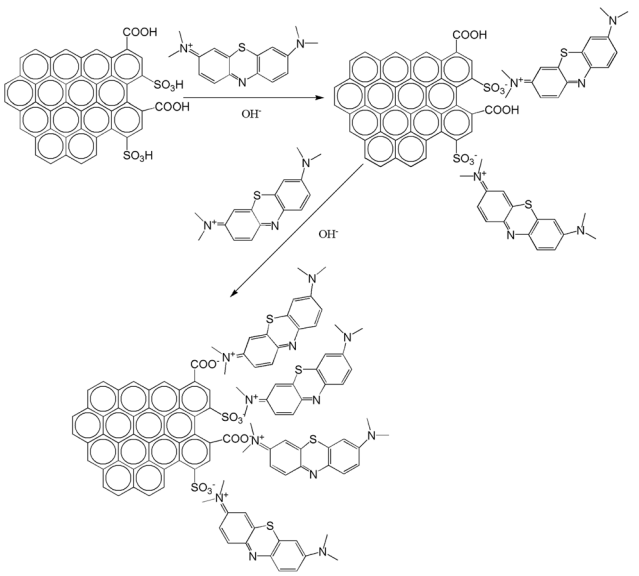

Fig. 10 Proposed schematic structure of AC-400 and its adsorption mechanism for MB.

AC-400 before and after adsorption were performed and presented in Fig. 9.

Fig. 9(a) showed that the absorbance of MB solution was greatly reduced after the adsorption. Fig. 9(b) showed that new peaks at 2890 cm^{-1}, 1490 cm^{-1} and 1330 cm^{-1} *etc.* appeared, compared with those of AC-400, indicating MB was successfully adsorbed on AC-400.[8] In addition, broad peaks at 3440 cm^{-1} and 1710 cm^{-1} weakened greatly after adsorption, demonstrating that the –COOH group in AC-400 has been transformed to the carboxylate form ($-COO^-$). Based on the above experimental results, the structure of AC-400 and its adsorption mechanism for MB were proposed in Fig. 10.

It can be observed from Fig. 10 that at low pH only $-SO_3H$ dissociated to $-SO_3^-$, which can attract the cationic dye MB by electrostatic forces. With the increase of pH, more and more –COOH were dissociated to $-COO^-$, and as a result, the adsorption capacity of AC-400 increased with increasing pH. Boehm titration has shown that the total amount of acidic functional groups in AC-400 is 7.63 mmol g^{-1}, which means that its adsorption capacity can reach 2441.6 mg L^{-1} (7.63 mmol g^{-1} × 320 mg $mmol^{-1}$ (molecular weight of MB) just by electrostatic interaction). However, Table 1 shows that maximum adsorption capacity of AC-400 is 2816 mg g^{-1}, which means that the other adsorption mechanism exists, although minor.

4 Conclusions

In this study, a high adsorption capacity AC was prepared by direct carbonization of the waste dried third-monomer press filtration liquid. The optimum carbonization temperature is 400 °C. The prepared AC at this carbonization temperature shows a porous structure and rich in carboxyl and sulfonic functional groups with disordered graphite-like crystal structure. The adsorption of AC for MB reaches equilibrium at 40 min and performs best at pH 12. The adsorption capacity increased with initial MB concentration and adsorption temperature. The adsorption is endothermic and spontaneous, conforms to the pseudo-second-order kinetics and Langmuir isotherm model. Strong static electric action between ionized carboxyl and sulfonic functional groups and cationic MB leads to its maximum adsorption capacity for MB reaching as high as 2816.4 mg g^{-1}, much higher than those reported to date. The present investigation opens a new way to treat the waste liquid.

Conflicts of interest

There are no conflicts to declare.

Acknowledgements

This work was supported by the National Natural Science Foundation of China (11005014, 11675031).

References

1 X. Wang, D. Wang, G. Cui, *et al.*, Study on the neutralization process in the production of dimethyl isophthalate-5-sulfonic acid sodium salt, *Shandong Chem. Ind.*, 2012, **41**(02), 5.
2 X. Guo, D. Xu, H. Guo, *et al.*, A method for extracting sodium isophthalate-5-sulfonate from wastewater from three monomer production, *Chinese Pat.*, 201410356437.9, 2014.
3 L. Chen, Study on pretreatment measures before biological treatment of industrial toxic organic wastewater, *Resources Economization & Environmental Protection*, 2015, (03), 108.
4 J. Yang, Q. Zhang, Y. Zhang, *et al.*, Method of extracting sodium isophthalate-5-sulfonate from third-monomer production wastewater, *Chinese Pat.*, 201410262626.X, 2014.
5 J. He, *Process design for resource treatment of three-monomer wastewater*, Nanjing Agricultural University, 2005.
6 M. Zhao, Y. Xiao, G. Gao, *et al.*, Research progress on resource utilization of dye intermediate wastewater, *Tianjin Chem. Ind.*, 2007, **21**(6), 4–7.
7 L. A. Yuan, W. A. Fei, A. Ym, *et al.*, A lignin-biochar with high oxygen-containing groups for adsorbing lead ion prepared by simultaneous oxidization and carbonization, *Bioresour. Technol.*, 2020, **307**, 123165.
8 F. Marrakchi, M. J. Ahmed, W. A. Khanday, *et al.*, *Int. J. Biol. Macromol.*, 2017, **98**, 233–239.
9 B. Sukhbaatar, B. Yoo and J. H. Lim, Metal-free high-adsorption-capacity adsorbent derived from spent coffee grounds for methylene blue, *RSC Adv.*, 2021, **11**(9), 5118–5127.
10 W. A. Khanday, M. J. Ahmed, P. U. Okoye, *et al.*, *Bioresour. Technol.*, 2019, **280**, 255–259.
11 G. Mohamed, O. El-Shafey and N. A. Fathy, *Egypt. J. Chem.*, 2017, **60**, 793–804.
12 H. A. S. Tohamy, N. A. Fathy, M. El-Sakhawy, *et al.*, Boosting the adsorption capacity and photocatalytic activity of activated carbon by graphene quantum dots and titanium dioxide, *Diamond Relat. Mater.*, 2023, **132**, 109640.

13 Y. Chen, J. Liu, Q. Zeng, *et al.*, Preparation of Eucommia ulmoides lignin-based high-performance biochar containing sulfonic group: Synergistic pyrolysis mechanism and tetracycline hydrochloride adsorption, *Bioresour. Technol.*, 2021, **329**, 124856.
14 W. A. Khanday, M. Asif and B. H. Hameed, Cross-linked beads of activated oil palm ash zeolite/chitosan composite as a bio-adsorbent for the removal of methylene blue and acid blue 29 dyes, *Int. J. Biol. Macromol.*, 2017, **95**, 895–902.
15 F. Arias and T. Sen, Removal of zinc metal ion (Zn^{2+}) from its aqueous solution by kaolin clay mineral: A kinetic and equilibrium study, *Colloids Surf., A*, 2009, **348**(1), 100–108.
16 A. K. Bhattacharya, S. N. Mandal and S. K. Das, Adsorption of Zn(II) from aqueous solution by using different adsorbents, *Chem. Eng. J.*, 2006, **123**(1–2), 43–51.
17 Y. Oenal, Kinetics of adsorption of dyes from aqueous solution using activated carbon prepared from waste apricot, *J. Hazard. Mater.*, 2006, **137**(3), 1719–1728.
18 S. S. Baral, S. N. Das, G. R. Chaudhury, *et al.*, Adsorption of Cr(VI) using thermally activated weed Salvinia cucullata, *Chem. Eng. J.*, 2008, **139**(2), 245–255.
19 T. H. Liou and S. J. Wu, Characteristics of microporous/mesoporous carbons prepared from rice husk under base- and acid-treated conditions, *J. Hazard. Mater.*, 2009, **171**(1–3), 693–703.
20 T. Lou, Development of mesoporous structure and high adsorption capacity of biomass-based activated carbon by phosphoric acid and zinc chloride activation, *Chem. Eng. J.*, 2010, **158**, 129–142.
21 P. Barpanda, G. Fanchini and G. Amatucci, Structure, surface morphology and electrochemical properties of brominated activated carbons, *Carbon*, 2011, **49**, 2538–2548.
22 Z. Zhang, K. Wang, J. Atkinson, *et al.*, Sustainable and hierarchical porous Enteromorpha prolifera based carbon for CO capture, *J. Hazard. Mater.*, 2012, (229–230), 183–191.
23 M. Goswami and P. Phukan, Enhanced adsorption of cationic dyes using sulfonic acid modified activated carbon, *J. Environ. Chem. Eng.*, 2017, **5**(4), 3508–3517.
24 D. Shen, J. Hu, R. Xiao, *et al.*, Separation and structural characterization of lignin in papermaking black liquor, *J. Southeast Univ.*, 2013, **43**, 12.
25 S. Wang, H. Lin, B. Ru, *et al.*, Comparison of the pyrolysis behavior of pyrolytic lignin and milled wood lignin by using TG–FTIR analysis, *J. Anal. Appl. Pyrolysis*, 2014, **108**, 78–85.
26 Y. Yang and F. S. Cannon, Biomass activated carbon derived from pine sawdust with steam bursting pretreatment; perfluorooctanoic acid and methylene blue adsorption, *Bioresour. Technol.*, 2022, **344**, 126121.
27 F. Yang, L. Sun, W. Zhang, *et al.*, One-pot synthesis of porous carbon foam derived from corn straw: atrazine adsorption equilibrium and kinetics, *Environ. Sci.: Nano*, 2017, **4**(3), 625–635.
28 M. Han, K. Jiang, P. Jiao, *et al.*, Bio-butanol sorption performance on novel porous-carbon adsorbents from corncob prepared via hydrothermal carbonization and post-pyrolysis method, *Sci. Rep.*, 2017, **7**(1), 11753.
29 H. Li, X. Ye, Z. Geng, *et al.*, The influence of biochar type on long-term stabilization for Cd and Cu in contaminated paddy soils, *J. Hazard. Mater.*, 2016, **304**, 40–48.
30 T. Wen, J. Wang, S. Yu, *et al.*, Magnetic porous carbonaceous material produced from tea waste for efficient removal of As(V), Cr(VI), humic acid, and dyes, *ACS Sustainable Chem. Eng.*, 2017, **5**(5), 4371–4380.
31 S. Suganuma, K. Nakajima and M. Kitano, *J. Am. Chem. Soc.*, 2008, **130**(38), 12787–12793.
32 S. Fan, J. Tang, Y. Wang, *et al.*, Biochar prepared from co-pyrolysis of municipal sewage sludge and tea waste for the adsorption of methylene blue from aqueous solutions: Kinetics, isotherm, thermodynamic and mechanism, *J. Mol. Liq.*, 2016, **220**, 432–441.
33 Y. S. Ho, Pseudo-second order model for sorption processes, *Process Biochem.*, 1999, **34**(5), 451–465.
34 D. Pathania, S. Sharma and P. Singh, Removal of methylene blue by adsorption onto activated carbon developed from Ficus carica bast, *Arabian J. Chem.*, 2017, **10**, S1445–S1451.
35 K. Hameed, P. Muthirulan and M. Sundaram, Adsorption of chromotrope dye onto activated carbons obtained from the seeds of various plants: Equilibrium and kinetics studies, *Arabian J. Chem.*, 2013, **153**(S2), 501–519.
36 Q. Wang, C. Luo, Z. Lai, *et al.*, Honeycomb-like cork activated carbon with ultra-high adsorption capacity for anionic, cationic and mixed dye: Preparation, performance and mechanism, *Bioresour. Technol.*, 2022, **357**, 127363.
37 A. Kumar and H. M. Jena, Removal of methylene blue and phenol onto prepared activated carbon from Fox nutshell by chemical activation in batch and fixed-bed column, *J. Cleaner Prod.*, 2016, **137**, 1246–1259.
38 B. Yang, Y. Liu, Q. Liang, *et al.*, Evaluation of activated carbon synthesized by one-stage and two-stage co-pyrolysis from sludge and coconut shell, *Ecotoxicol. Environ. Saf.*, 2019, **170**, 722–731.
39 P. Zhang, D. O'Connor, Y. Wang, *et al.*, A green biochar/iron oxide composite for methylene blue removal, *J. Hazard. Mater.*, 2020, **384**, 121286.1–121286.8.